J. Fluid Mech. (1993), *vol.* 254, *pp.* 375–400

The Rayleigh–Bénard problem in intermediate bounded domains

By F. STELLA[1], G. GUJ[1] AND E. LEONARDI[2]

[1] Dipartimento di Meccanica e Aeronautica, Università degli Studi di Roma 'La Sapienza', Via Eudossiana 18, 00184 Rome, Italy

[2] The University of New South Wales, Kensington, NSW, Australia 2033

(Received 20 May 1991 and in revised from 21 February 1993)

The stationary instabilities of flow patterns associated with Rayleigh–Bénard convection in a $3 \times 1 \times 9$ rectangular container are extensively investigated by numerical simulation. Two types of spatial instabilities of the base convection rolls are predicted in the transition from steady two-dimensional flow to the unsteady oscillatory regime; these instabilities depend on the Prandtl number. For $Pr = 0.71$ the *soft-roll* instability is found at moderate Rayleigh number Ra. The results obtained confirm the importance of this flow pattern as a continuous mechanism for steady transition from one wavenumber to another. For $Pr = 15$, *cross-roll* instability is obtained, which at larger Ra leads to *bimodal convection*. For this value of Pr the soft-roll flow pattern is found at intermediate Ra. At higher Ra a new flow structure in which cross-rolls are superimposed on the soft roll is obtained. The effects of the various flow structures on the heat transfer are given. A quantitative comparison with previous experimental and theoretical findings is also presented and discussed.

1. Introduction

Natural convection in a layer heated from below has been extensively studied during the past century, beginning with the experiments of Bénard (1900*a*, *b*) and the theoretical analysis of Rayleigh (1916).

Two different aspects have contributed to the interest in this problem: first, there are many practical applications such as thermal comfort, crystal growth and solar collectors, which depend on this type of convection; the second aspect is theoretical since a variety of different flow structures may occur, in this very simple geometry, in the transition from steady laminar to turbulent flows.

A large scientific effort has been devoted to the analysis of the stability and behaviour of fluid layers of infinite horizontal extent. The dependence of the flow configuration on Prandtl (Pr) and Rayleigh numbers (Ra) and the shape of the stability region in the (Ra, wavenumber)-plane is widely known and described in both theoretical (Busse 1967*a*) and experimental papers (Busse & Whitehead 1971).

Studies of infinite domains also play an important role in the prediction of flow in bounded domains, particularly at values of Ra near the first critical value Ra_I. It has been shown (Davies 1967; Davies-Jones 1970; Stork & Müller 1972) that the value of Ra_I itself, which is 1708 and corresponds to the onset of cellular convection, is insensitive to aspect ratio (for aspect ratios greater than 2) and independent of Pr. In the supercritical-Ra region however, the structures in bounded domains are strongly affected by the geometry of the box and thermal properties of the sidewalls (Kessler 1987) as well as by the physical characteristics of the fluid. In these regions of Ra the

infinite analysis can only be used for qualitative comparisons and preliminary estimates of the critical values of the governing parameters for transition between flow regimes.

In the last decade there has been renewed interest in the problem of spatial and temporal instabilities of fully developed three-dimensional flow structures (Kolodner *et al.* 1986; Kessler 1987; Kirchartz & Oertel 1988). Of particular interest is the complex scenario which is possible in the supercritical regime due to the important role played by *Pr*. This is analogous to the behaviour that occurs in unbounded domains as observed experimentally by Krishnamurti (1970).

We have thus undertaken a numerical study of Rayleigh–Bénard convection in a bounded domain in relation to the slope and characteristics of the stability regions of the different flow structures, selecting two *Pr* values (0.71 and 15), which are significantly different.

Let us first consider $Pr = 0.71$ (air at 15 °C).

(i) From the stability diagram (figure 2 of Busse & Clever 1979) for an infinite layer, it is seen that there is a very thin stability region (maximum Ra_{II} for the stable configuration is approximately 6000), bounded by the skewed-varicose instability (which corresponds to a periodic thickening and thinning of the convection rolls) for a wavenumber α larger than 2.3 and by the oscillatory instability for α less than 2.3. (The wavenumber is defined as $\alpha = 2\pi/l$, where l is the wavelength.) This is contrasted by the results of Kessler (1987) who solved the Boussinesq equations using a Galerkin method and obtained $Ra_{II} = 33400$ in a $4 \times 2 \times 1$ box ($\alpha = 2.35$, n (number of rolls) = 3) and by those of Kirchartz & Oertel (1988), who, using a finite-difference method based on the Dufort–Frankel scheme in the same box, obtained $Ra_{II} = 34000$. These values are approximately six times larger than expected from the theoretical study of an infinite layer (Busse & Clever 1979). This has been attributed to sidewall effects (Motsay, Anderson & Behringer 1988). Maurer & Libchaber (1979) experimentally found $Ra_{II} = 23500$ for the same *Pr*, in a $3.5 \times 1.9 \times 1$ box.

(ii) The experimental investigations as well as the theoretical studies of Busse & Clever (1979) in an unbounded domain have shown that the skewed varicose instability is a basic mechanism for the quasi-steady modification of the wavelength as a function of *Ra*. On the other hand, in limited domains the modification of the wavenumber is driven by a different type of spatial instability, which has become known as a soft roll. This has been experimentally investigated in a $10 \times 5 \times 1$ box by Kolodner *et al.* (1986). They found a T-shaped-roll which can be squeezed or stretched, resulting in a modification of the wavenumber required by the stability boundary. None of the previous available numerical results have shown a spatial instability of the skewed-varicose or soft-roll type. In particular Kirchartz & Oertel (1988) state that 'the modification of the wavelength, which develops in discrete steps in the container as a result of the finite number of rolls, cannot be satisfactorily described by the numerical simulation'.

For intermediate and high *Pr* (> 10) Busse & Whitehead (1971) observed experimentally, and Busse (1967*a*) and Frick, Busse & Clever (1983) studied theoretically, the cross-roll instability leading to a transition to bimodal convection. There is experimental evidence that this kind of instability also occurs in limited domains (Kolodner *et al.* 1986). However, to date none of the numerical studies provided a detailed investigation of the cross-roll flow configuration in enclosures of limited dimensions.

In the present work a systematic numerical study is presented of the three-dimensional flow and thermal fields in a $3 \times 1 \times 9$ box ($l_1 = L/H$, $l_2 = 1$, $l_3 = W/H$, see figure 1) heated from below and with adiabatic lateral walls. Like Kolodner *et al.*

(1986), we were motivated in the choice of these aspect ratios by the desire to have a container sufficiently large to permit the observation of the onset of spatial flow patterns but sufficiently small to inhibit slow wandering of the rolls.

The numerical code used in this work is based on the vorticity–velocity formulation of the Navier–Stokes equations (Guj & Stella 1988, 1993) applied to a staggered uniform grid, which for the full domain typically contains $30 \times 20 \times 90$ mesh points.

The computed results confirm some interesting types of behaviour of the confined flows as discussed above, particularly: (i) multiplicity of solutions and flow structures for a given Ra; (ii) the existence of the soft-roll instability as a mechanism for the steady transition from one wavenumber to another at low Pr; (iii) qualitative agreement in the (Ra, α)-plane between the theoretical prediction of skewed-varicose instability and computed results of the soft roll – this seems to confirm that these structures are two forms of the same instability; (iv) the occurrence of the cross-roll instability leading to bimodal convection for intermediate Pr and high Ra.

2. Mathematical formulation

The vorticity–velocity form of the non-dimensional equations governing natural convection in a Newtonian fluid, assuming the Boussinesq approximation to be valid, are

$$\frac{1}{Pr}\frac{\partial \boldsymbol{\omega}}{\partial t}+\frac{1}{Pr}\boldsymbol{\nabla}\times(\boldsymbol{\omega}\times\boldsymbol{u}) = \nabla^2\boldsymbol{\omega}-Ra\,\boldsymbol{\nabla}\times\left(\theta\frac{\boldsymbol{g}}{g}\right), \tag{1}$$

$$\boldsymbol{\nabla}^2\boldsymbol{u} = -\boldsymbol{\nabla}\times\boldsymbol{\omega}, \tag{2}$$

$$\frac{\partial\theta}{\partial t}+(\boldsymbol{u}\cdot\boldsymbol{\nabla})\,\theta = \nabla^2\theta, \tag{3}$$

in which θ is the non-dimensional temperature $= (T-T_c)/\Delta T$, and $Ra = g\beta\Delta T H^3/\kappa\nu$ and $Pr = \nu/\kappa$ are the Rayleigh and Prandtl numbers respectively, where g is the modulus of the gravitational acceleration, β is the coefficient of thermal expansion, H and ΔT are the distance and temperature difference between the hot and cold surfaces respectively, κ is the thermal diffusivity and ν is the kinematic viscosity.

The vorticity $\boldsymbol{\omega}$ is defined as

$$\boldsymbol{\omega} = \boldsymbol{\nabla}\times\boldsymbol{u}. \tag{4}$$

3. Boundary conditions

All boundaries of the box are assumed to be impermeable and at rest, $\boldsymbol{u} = 0$. The boundary conditions for vorticity are obtained directly from the definition of vorticity, (4).

The temperature boundary conditions are

$$\frac{\partial\theta}{\partial n} = 0, \quad \begin{cases} x_1 = 0, & l_1 \\ x_3 = 0, & l_3 \end{cases}$$

on the adiabatic walls, where n is the normal direction and

$$\theta = 1, \quad x_2 = 0,$$
$$\theta = 0, \quad x_2 = l_2$$

on the isothermal horizontal walls. Figure 1 shows the boundary conditions, locations and directions of the axes.

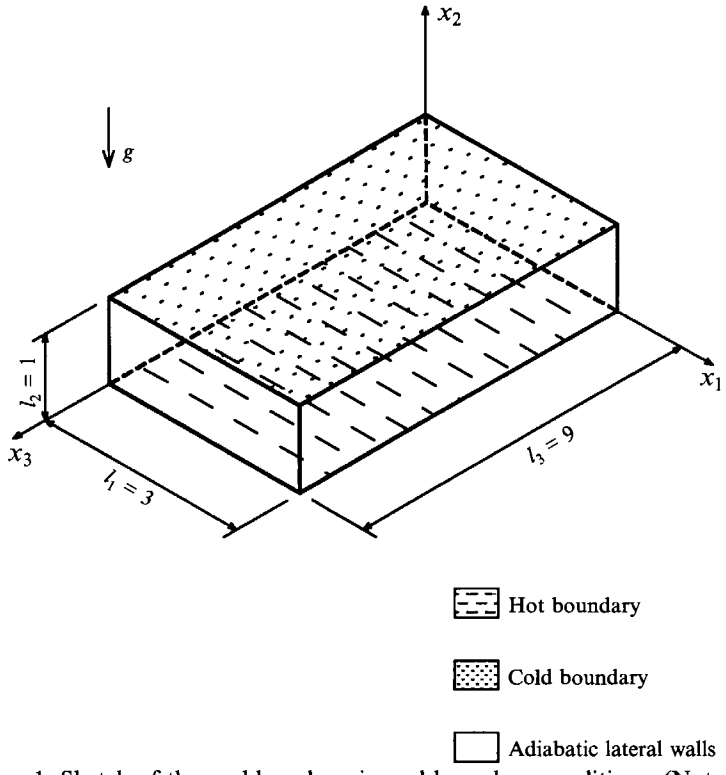

FIGURE 1. Sketch of the problem domain and boundary conditions. (Note that all boundaries are impermeable and non-slip.)

4. Numerical procedure

4.1. *Finite-difference scheme and convergence criterion*

The governing equations (1)–(3) were discretized by a finite-difference approximation (FDA) on a regular Cartesian mesh with a second-order-accurate scheme for both time and space derivatives. Second-order accuracy in space is achieved by central differences for both first and second derivatives and second-order accuracy in time is obtained by adopting the Samarskii–Andreyev scalar-type alternating direction implicit (ADI) scheme (Samarskii & Andreyev 1963). This scalar-type ADI scheme permits appropriate timescales to be chosen for the different equations to speed up the convergence of the numerical procedure when steady-state solutions are sought (Mallinson & de Vahl Davis 1973).

The convergence criterion was based on the field-averaged dynamical residual which had to be less than 10^{-6} on (1)–(3); then the quality of convergence at steady state was checked by the calculation of the maximum absolute error (static residuals) of the steady-state form of (1)–(3) as well as on the equations that are only implicitly solved in the present formulation, viz, vorticity definition (4) and solenoidality of velocity $\boldsymbol{u}$ and vorticity $\boldsymbol{\omega}$ fields. These residuals were required to be less than 10^{-4}, otherwise the computation was forced to continue.

4.2. *Conservation properties and variables location*

The staggering of the variable location was chosen not only to obtain the maximum accuracy of the discretized derivatives but also to ensure the discrete conservation of mass, vorticity and thermal energy. By analogy with the two-dimensional case (Guj &

Stella 1988), it is possible to obtain mass conservation, to round-off error, if the velocity component u_i is located at the middle of the face of the computational cell which is normal to x_i. Similarly, conservation of vorticity is achieved if each vorticity component is located at the midpoint of the edge of the cell parallel to the corresponding axis.

Some additional remarks are necessary to explain the form of the advective term in (1). First, we demonstrate that (1) implicitly enforces the solenoidality of vorticity $\boldsymbol{\omega}$ at continuum level. Denoting the divergence of vorticity $\nabla\cdot\boldsymbol{\omega}$ by D and taking the divergence of (1), we obtain a diffusion equation for the divergence of the vorticity:

$$\frac{1}{Pr}\frac{\partial D}{\partial t} = \nabla^2 D. \tag{5}$$

It follows that the solenoidality of the vorticity field is ensured, provided that $D = 0$ on all boundaries. Secondly it can be demonstrated (Guj & Stella 1993) by discrete manipulation of (5) that the solenoidality of the vorticity field is also ensured in the discrete form provided that the variables are staggered as mentioned above, and that in obtaining the FDA for the advective terms $\nabla\times(\boldsymbol{\omega}\times\boldsymbol{u})$ all required averaging is performed on the product $(\boldsymbol{\omega}\times\boldsymbol{u})$ rather than on the individual values of $\boldsymbol{\omega}$ and $\boldsymbol{u}$.

Finally, for energy conservation, the temperature has been located at the centre of the cell in analogy with the work of Stella & Guj (1989). Here the convective term in (3) has been discretized in such a way that the quantity $\int_s(\theta\boldsymbol{u}-\nabla\theta)\cdot\boldsymbol{n}\,\mathrm{d}s$ (s is the surface of a cell) vanishes. Consequently, the variable location and discretization form give the best conservation of energy, so that the mean Nusselt number on a horizontal section of the fluid domain, defined as

$$Nu = \frac{1}{S}\int_S (\theta\boldsymbol{u}-\nabla\theta)\cdot\boldsymbol{n}\,\mathrm{d}S \tag{6}$$

is constant and equal to Nu on the bottom and top walls.

4.3. *Computational mesh and accuracy*

The box is discretized using a uniform grid which typically contains $30\times20\times90$ mesh points. A uniform grid has been preferred for the following reasons: (i) it guarantees second-order accuracy, which is important in reducing numerical viscosity and dissipation, both of which can adversely modify the transition mechanism between the various flow patterns in stability studies; (ii) due to the multiple-cell structure the high-gradient regions (of velocity and temperature) are located not only near the walls, but also in the bulk of the fluid in positions determined by the cellular structure itself which is not known *a priori*. It should be noted that in order to reduce the CPU time and storage requirements symmetric boundary conditions have been used where possible, to reduce the computational domain to one half or one quarter of the total region of interest. The correctness of the numerical solutions obtained using such reduced computational domains was validated by comparing a number of such solutions with solutions for the entire domain.

The capability of the method in computing the complex three-dimensional flow structures of the Rayleigh–Bénard problem is demonstrated by comparison with the experimental results of Kolodner *et al.* (1986). The details of mesh sensitivity and accuracy are deferred to §5.2, because knowledge is required of the complex flow structures present in this type of flow. Various preliminary accuracy tests of the method

were conducted by comparisons with vorticity-vector potential formulations (Mallinson & de Vahl Davies 1977) for the standard window cavity problem and are presented in Stella *et al.* (1988).

4.4. *Initial condition*

As observed by Landau & Lifshitz (1975, p. 102) every solution of the equation of motion which is stable can also occur in nature, irrespective of the solution method used. Hence, for fixed physical boundary conditions, the initial condition plays the only important role in starting the solution from a point which is within the attraction basin of the numerical procedure for a certain structure. In our experience this can be done by imposing as a starting solution a vorticity distribution approximately similar to the one which is expected as the final one.

The following different strategies have been used: (i) an initial inclination of the box is used to induce a vorticity distribution in the desired direction (see e.g. Kirchartz & Oertel 1988); (ii) a change in aspect ratio is used to control the initial number of rolls (i.e. wavenumber), since the smaller the aspect ratio the smaller the number of rolls because for Ra just above Ra_I the natural structure is the one with parallel rolls of nearly square section; (iii) starting from a solution at different Ra or Pr values; (iv) low Ra starting from rest, where most of the quasi-two-dimensional natural structures (with near square cross-section) have been obtained. The steady-state solution is reached after the enforcement of the prescribed geometry and physical parameters.

4.5. *Evaluation of* Ra_{II}

The critical Ra for transition to oscillatory solutions (Ra_{II}) is evaluated by incrementing the value of Ra until an unsteady solution is found. In the neighbourhood of Ra_{II} the amplitude of the oscillatory solution is proportional to $(Ra-Ra_{II})^{\frac{1}{2}}$ (Joseph 1976), resulting in a gradual transition from a steady to a finite-amplitude oscillatory region. For this reason all the numerical solutions, as well as experimental observations, are affected by an overestimation of Ra_{II}, proportional to the square of the uncertainty of the observed field variables. In this work, for solutions which we considered to be numerically unsteady, no noticeable change was found in the flow structure and the qualitative variations of the field variables evaluated in the complete fluid domain are very small. We believe it is for this reason that some other numerical or experimental studies have overestimated values for Ra_{II}.

Although a systematic study of Ra_{II} has not been fully conducted, due also to the enormous computational requirements in terms of both computer time and memory for three-dimensional mesh refinements, we are able to give (see §5) some indicative values of the critical Ra_{II}.

5. Results

In the present work we have examined qualitatively and quantitatively the flow and thermal fields in a $3.0 \times 1.0 \times 9.0$ box in the steady supercritical regime $Ra_I < Ra < Ra_{II}$ for $Pr = 0.71$ and 15.

Different geometrical and physical situations are also considered and briefly discussed in §5.2 to test the accuracy of the proposed numerical model and to investigate some interesting results which have appeared in the literature (Kolodner *et al.* 1986; Kessler 1987).

5.1. *General discussion*

As discussed by many authors (Davies 1967; Davies-Jones 1970; Stork & Müller 1972) the value of $Ra_I = 1708$, corresponding to the onset of cellular convection, is independent of Pr and weakly sensitive to aspect ratio (for aspect ratio greater than 2).

The steady supercritical regime, which appears at increasing Ra ($Ra_I < Ra < Ra_{II}$), can be subdivided into two flow regimes:

(i) Quasi-two-dimensional motion in the form of periodic nearly rectilinear rolls, comprising either: 8 transverse rolls (8T), which are orthogonal to the longest sidewall of the box, with $\alpha = 2.79$; 6 transverse rolls (6T) with $\alpha = 2.09$; 3 longitudinal rolls (3L), which are parallel to the longest sidewall of the box with $\alpha = 3.14$; or 2 longitudinal rolls (2L) with $\alpha = 2.09$.

(ii) Fully three-dimensional flow caused by: bimodal convection, comprising of a base flow superimposed with cross-rolls of approximately the same strength as the base flow (cross-roll instability); or distortion of the original roll in soft form during the quasi-steady transition from one configuration to another with a smaller wavenumber (skewed-varicose instability).

For the supercritical regime, it has been demonstrated theoretically by Busse & Clever (1979) and shown experimentally (e.g. Krishnamurti 1970, figure 9) that the flow structure, the type of spatial instability and the transition to periodic motion strongly depends on Pr. For this reason we have analysed separately cases at a low ($Pr = 0.71$) and intermediate Pr ($Pr = 15$).

In discussing the numerical results obtained in the present analysis we refer to the stability studies and diagrams for an infinite layer of fluid (Busse 1967*b*; Clever & Busse 1974; Busse & Clever 1979; Kolodner *et al.* 1986; Bolton, Busse & Clever 1986). In these studies the base steady two-dimensional solution was obtained by expanding the unknowns in terms of eigenfunctions. The stability problem was investigated by superimposing infinitesimal disturbances of arbitrary three-dimensional spatial dependence to the base solution. By this method the stability diagrams of figure 2 of Busse & Clever (1979) and figure 2 of Kolodner *et al.* (1986)† were obtained. We have superimposed our results on these diagrams in the plane (Ra/Ra_I, α) for $Pr = 0.71$ and 15 (figures 2 and 3 respectively). It should be noted that the zig-zag instability cannot appear in the case of limited domains because of the straightening effect of the lateral walls (Busse & Whitehead 1971). On the other hand, a form of skewed-varicose instability, which corresponds to a periodic thickening and thinning of the convection rolls, might also be expected to exist in limited domains, since it is an instability of this type which results in the steady transition from a higher to a more stable lower wavenumber flow structure.

5.2. *Preliminary study*

Before considering in detail the $3.0 \times 1.0 \times 9.0$ geometry, a preliminary study is presented to (i) validate the numerical method by comparison with experimental results and by a mesh sensitivity analysis, and (ii) further discuss the results of Kolodner *et al.* (1986) and Kessler (1987).

5.2.1. *Validation of the numerical method*

Two test cases have been chosen in order to justify the grid adopted in the final computations and to validate the results of the present numerical experiments with previous experimental investigations:

† As noted by Kolodner *et al.* (1986), the stability boundaries presented in their figure are interpolated and extrapolated from the calculations of Busse & Clever (1979), Busse (1978), and Bolton, Busse & Clever (1983).

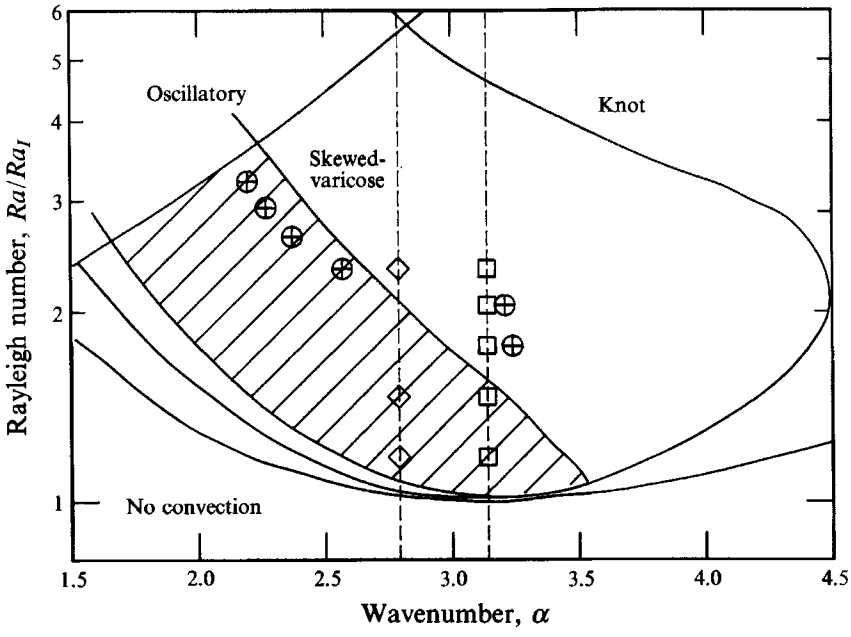

FIGURE 2. Present numerical results, for $Pr = 0.71$ superimposed on the stability diagram of Busse & Clever (1979), for an infinite domain. For the soft roll α is computed using the dimension of the central transverse roll. The soft-roll results (⊕) follow the skewed-varicose stability line. The 3L configuration (□) seems more stable than the prediction for an infinite domain. The 8T configuration is denoted ◇.

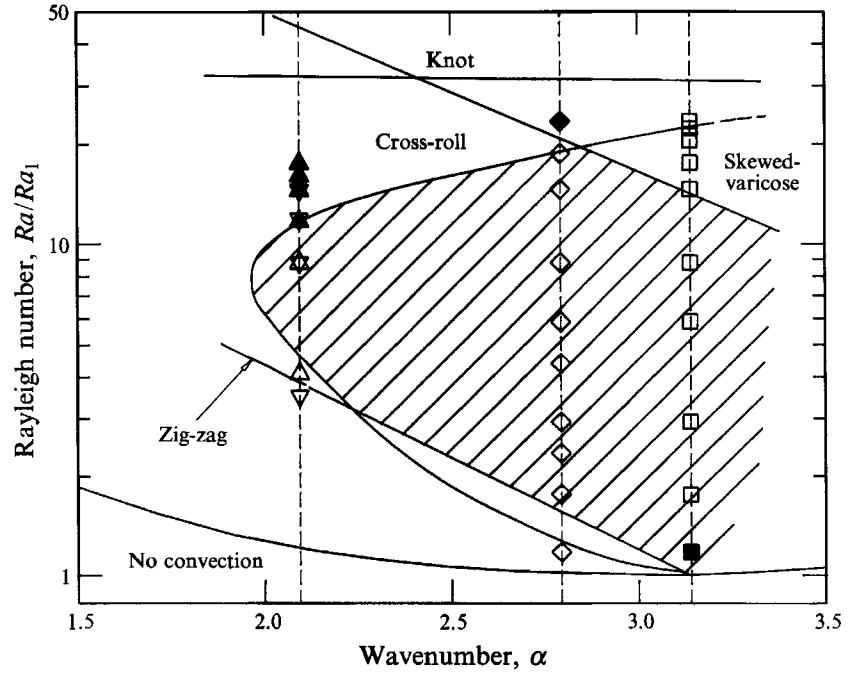

FIGURE 3. Present numerical results, for $Pr = 15$, superimposed on the stability diagram (Kolodner *et al.* 1986) in the case of infinite domain. The cross-roll structures (filled symbols) are found at Ra/Ra_1 whose difference from the theoretical prediction is less than 15%, which is of the order of the uncertainty stated by Kolodner *et al.* (1986). ◇, 8T configuration; △, 6T; □, 3L; ▽, 2L.

Mesh type	DOF	Structure	H_1 (error %)	H_3 (error %)	V_{2M} (error %)	Nu (error %)
A	51408	SCR	0.520	1.085	76.77	2.850
			(2.8)	(3.9)	(0.5)	(6.9)
B	108192	SCR	0.536	1.121	77.07	2.756
			(0.3)	(0.7)	(0.1)	(3.4)
C	219240	SCR	0.536	1.126	77.21	2.708
			(0.2)	(0.3)	(0.1)	(1.6)
D	432432	SCR	0.536	1.131	77.03	2.680
			(0.3)	(0.2)	(0.2)	(0.6)
E	844928	SCR	0.535	1.129	77.16	2.665
			(—)	(—)	(—)	(—)

TABLE 1. Mesh sensitivity to degrees of freedom. Mesh types are: A ($12 \times 17 \times 36$), B ($16 \times 21 \times 46$), C ($20 \times 27 \times 58$), D ($26 \times 33 \times 72$), E ($32 \times 41 \times 92$). H_1 and H_3 are the characteristic lengths of the transverse central and soft roll respectively. V_{2M} is the maximum vertical velocity and Nu is the Nusselt number on a horizontal plane. Mesh B is the standard grid used for the computations on a quarter of the domain.

(i) The standard $3 \times 1 \times 9$ box, for $Pr = 15$ and $Ra = 17000$ – selected for the mesh sensitivity analysis because at these parameter values the most complex flow structures, namely soft cross-rolls (SCR) are found. The mesh on a quarter of the domain is varied from $12 \times 17 \times 36$ to $32 \times 41 \times 92$ corresponding to a number of degree of freedom (DOF) from 51408 to 844928. The results of the mesh sensitivity analyses are presented in table 1, in terms of flow structures, the maximum vertical velocity and the global Nu on a horizontal plane. The structures obtained with the coarsest and finest meshes indicate that there is no perceptible modification for a change in the DOF of more than an order of magnitude. Further the dimension of the central transverse roll (H_3) and of the soft roll (H_1), shown in table 1 and defined in figure 4(*b*), changes by around 1 % between the standard grid used for the computations (108192 DOF) and the finest mesh.

(ii) A $4.4 \times 1 \times 9.3$ box which has the same geometry as container A of Kolodner *et al.* (1986), for $Pr = 5.5$ and a wide range of Ra. This was chosen so as to be able to quantitative compare, in terms of Nu, the results of Kolodner *et al.* (1986) with the present results. The numerically determined Nu numbers for the 8T and 10T configurations are superimposed on those of figure 10 of Kolodner *et al.* (1986) in figure 5, showing an error less than 4 % for the Ra considered.

5.2.2. *Some remarks concerning existing results*

In §1 we focused our attention on two aspects which required further discussion, namely (i) the capability of numerical codes to satisfactory simulate soft-roll structures, and (ii) Ra_{II} in small-aspect-ratio boxes. We have therefore selected and studied the following two cases for this discussion.

(i) A $5.3 \times 1 \times 10.6$ box, which has the same geometry as container B of Kolodner *et al.* (1986), for $Pr = 18$ and $Ra/Ra_I = 2.7$. This Ra is in the lower region of Ra in which Kolodner *et al.* (1986) found the soft-end-roll configuration. In figure 6(*a*) a contour plot of vertical velocities is shown at $Ra/Ra_I = 2.7$. The soft-roll configuration is clearly evident. In figure 6(*c*) the same result is presented in the form of a numerical shadowgraph, obtained by the vertical integration of the two-dimensional Laplacian of the temperature field on the horizontal planes, and is compared with the shadowgraph obtained by Kolodner *et al.* (1986), see figure 6(*b*). The agreement in flow

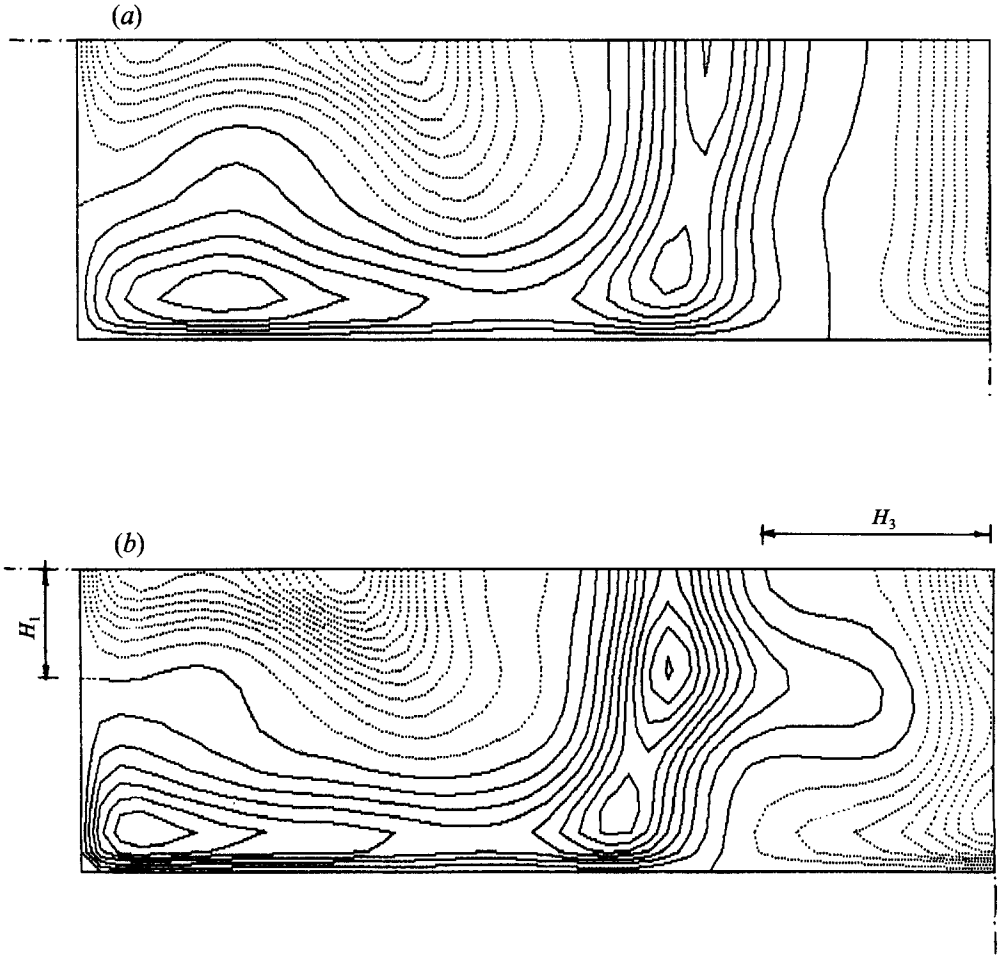

FIGURE 4. Contour plots of vertical velocity in the plane $x_2 = 0.5$ for soft-roll patterns at $Pr = 15$: variation of the shape of the soft rolls from $Ra = 12000$ (*a*) to 17000 (*b*). The simultaneous presence of the cross-roll may be seen at $Ra = 17000$. Continuous lines represent positive velocities and dashed lines represent negative velocities. (symmetry is assumed only for plotting.)

structure is very good. This result confirms the capability of the present numerical method to find, with good accuracy, complex flow structures and validates, from the numerical point of view, the existence and steadiness of the soft rolls found by Kolodner *et al.* (1986) in experiments where the physical parameters could not be controlled as well as in the numerical simulation.

(ii) The small-aspect-ratio box $2 \times 1 \times 4$ for $Pr = 0.71$ which has the same geometry as investigated by Kessler (1987). For $\alpha = 2.35$ we have found a steady solution for $Ra = 25000$ and a weakly oscillatory solution for $Ra = 27500$, which is lower than 33400 found by Kessler (1987) for the same flow configuration. However, it should be noted that Kessler (1987) determines Ra_{II} only by checking the amplification or damping of field-variable oscillations. The value estimated in the present research is in reasonable agreement with Ra_{II} ($= 23500$), for $\alpha = 1.79$, found experimentally by Maurer & Libchaber (1979) in a box $1.9 \times 1 \times 3.5$ at the same Pr. The present results confirm the strong effect of sidewalls as observed by Motsay *et al.* (1988).

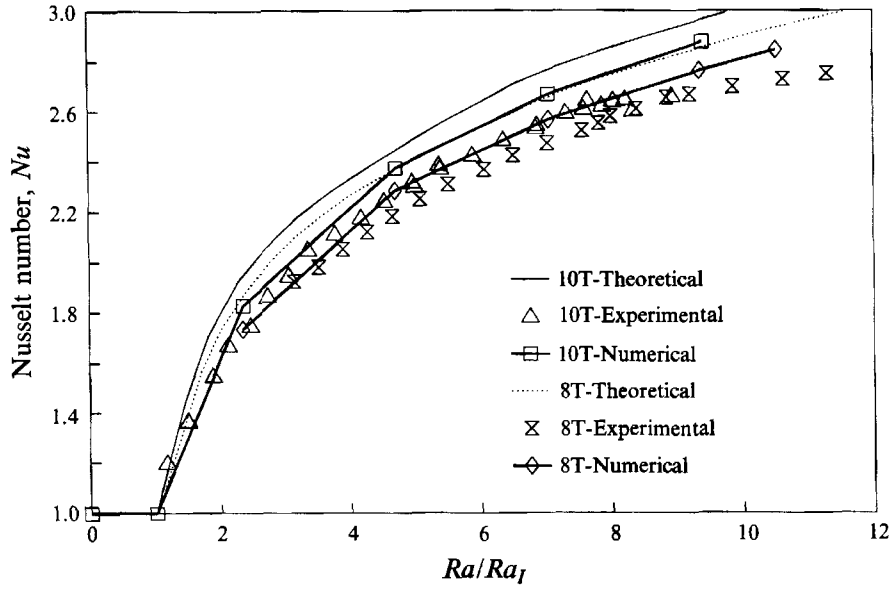

FIGURE 5. Comparison of Nu between the present numerical results and the experiments of Kolodner *et al.* (1986) in a $4.4 \times 1 \times 9.3$ container at $Pr = 18$ for the 8T and 10T configurations. The theoretical values for an infinite domain (Clever & Busse 1974) at the same Pr are also shown.

5.3. *Prandtl number* = 0.71

5.3.1 *Quasi-two-dimensional configurations*

Let us first consider the base quasi-two-dimensional pattern. Owing to the small size of the stability region (figure 2), in the case of $Pr = 0.71$ only 8T and 3L configurations have been found to be stable. The general discussion on the base quasi-two-dimensional solutions is deferred to the next section, since $Pr = 15$ offers a larger stability region and a more extensive picture of the base structures can be presented. Nevertheless, some preliminary comments, which refer only to $Pr = 0.71$ are necessary.

It should be noted that although stable solutions for $\alpha = 2.09$ (6T and 2L) are obtained for $Pr = 15$, they cannot be obtained for $Pr = 0.71$. This is probably due to the smaller dimension of the stability region for the latter (figures 2 and 3) combined with the wall effect, which affects the vorticity components perpendicular to the axis of the main rolls. To verify this hypothesis, we have approximated the flow in a box of infinite dimension in the direction of the axis of the 6T rolls ($\infty \times 1 \times 9$), by a very long ($40 \times 1 \times 9$) three-dimensional box with slip conditions on the endwalls. The resulting 6T structure is stable in accordance with figure 2. This structure remained stable as the aspect ratio was slowly decreased to ($14 \times 1 \times 9$). Below this aspect ratio no stable solution could be found, and it is believed that the endwall effect reduces the stability for the transition to the oscillatory solutions.

5.3.2. *Soft roll*

It may be seen from figure 2 that an increase in Ra leads to two types of instability. The first is a direct transition to oscillatory flows for $\alpha < 2.2$. This flow will not be discussed in the present paper since we are only interested in steady solutions. The second is the skew-varicose instability for $\alpha > 2.2$, which in bounded domains occurs

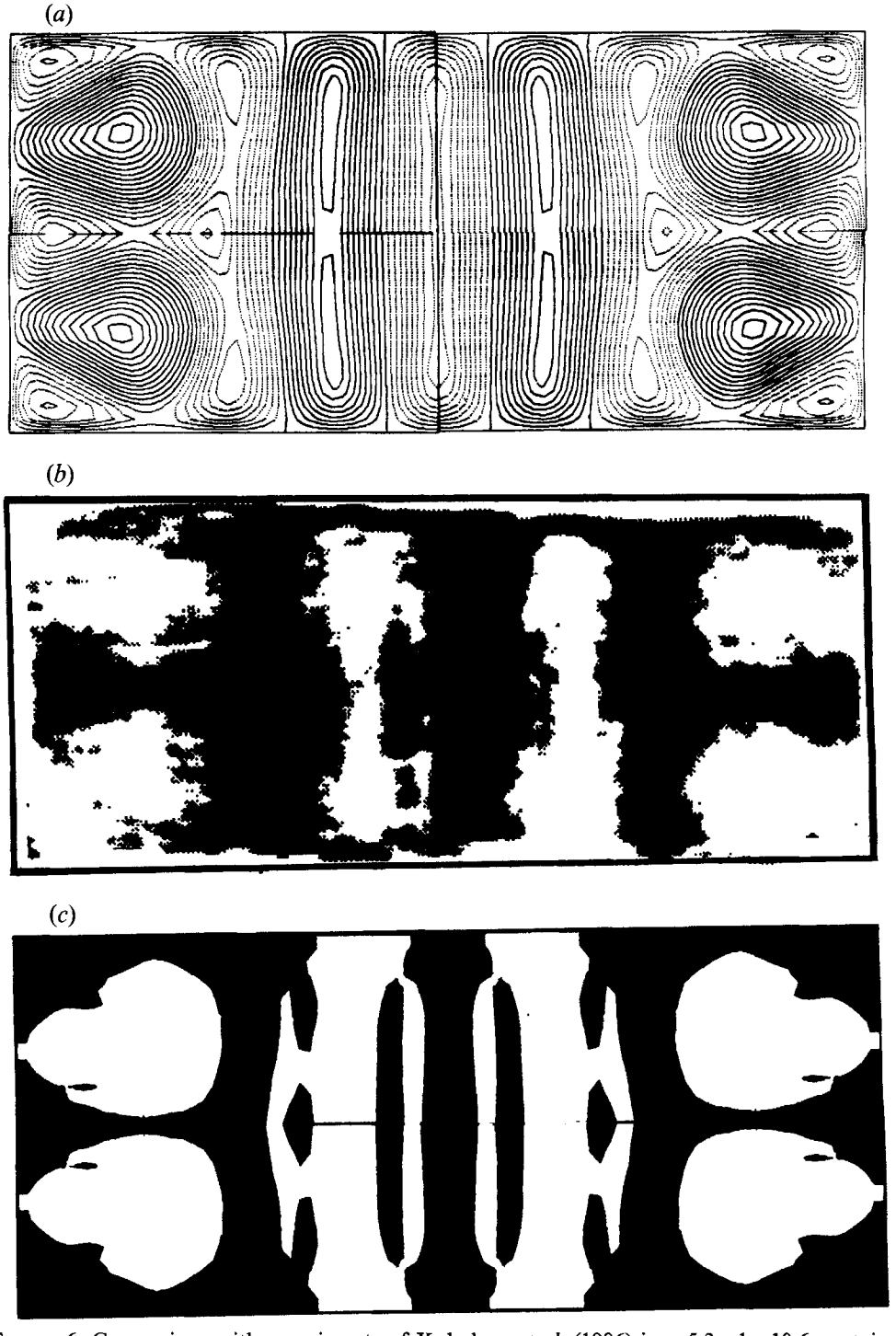

FIGURE 6. Comparison with experiments of Kolodner *et al.* (1986) in a $5.3 \times 1 \times 10.6$ container at $Ra/Ra_1 = 2.7$ and $Pr = 18$: (*a*) contour plot of vertical velocity in the plane $x_2 = 0.5$, (*b*) shadowgraph image obtained by Kolodner *et al.* (1986), (*c*) numerical simulation of the shadowgraph effect.

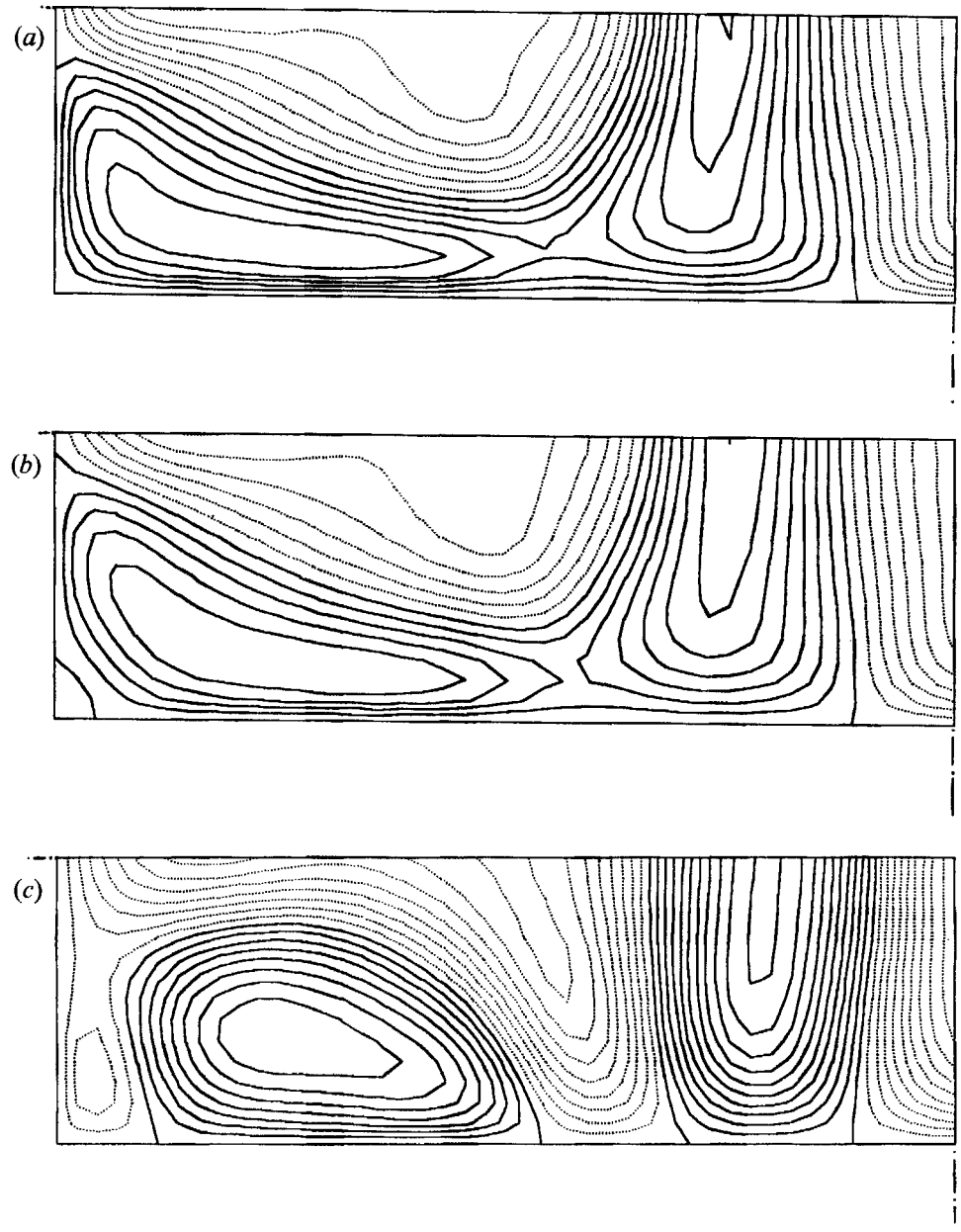

FIGURE 7. Contour plots of vertical velocity in the plane $x_2 = 0.5$ for soft-roll patterns at $Pr = 0.71$: variation of the shape of the soft rolls for $5500 \geqslant Ra \geqslant 3000$. Continuous lines represent positive velocities and dashed lines represent negative velocities. (Computations have been carried out on the full domain. symmetry is assumed only for plotting.) (*a*) $Ra = 5500$, (*b*) $Ra = 4500$, (*c*) $Ra = 3000$.

in the form of a soft roll (Kolodner *et al.* 1986). This last instability, in an infinite domain, corresponds to a spatially periodic thickening and thinning of the convection rolls, resulting in a tendency to eliminate the large-wavenumber rolls, leaving the low-wavenumber rolls (Busse & Clever 1979). The skewed-varicose instability cannot occur

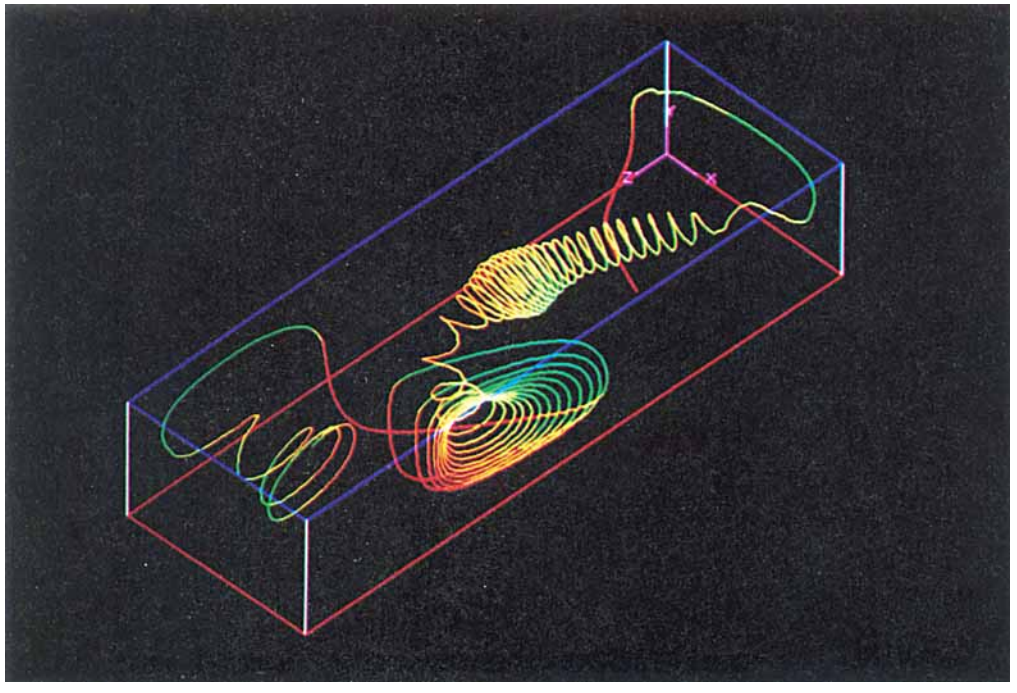

FIGURE 8. Soft-roll configuration: particle path ($Pr = 0.71$ and $Ra = 5000$). (Computations have been carried out on the full domain. symmetry is assumed only for plotting.)

	Transverse		Longitudinal	
Configuration	8T	6T	3L	2L
Wavenumber of the base flow, α	2.79	2.09	3.14	2.09
Ra ($\times 10^{-3}$) for transition to cross-roll:				
Infinite domain (Kolodner *et al.* 1986)	32	19	37	19
Present analysis	$32 \sim 40$	$15 \sim 20$	—	$20 \sim 25$
Wavenumber of cross-rolls, α_c	6.28	4.18	2.79	4.88
Occurring at Ra ($\times 10^{-3}$)	40	$20 \sim 30$	2	25
Wavenumber ratio, α_c/α	2.25	2.00	0.89	2.33
Ra ($\times 10^{-3}$) for transition to oscillatory solutions:				
Present analysis	> 40	> 30	> 40	> 25

TABLE 2. Critical Ra for the transition to cross-roll and oscillatory solutions, wavenumbers associated with the base and cross-rolls

in the form discussed by Busse & Clever (1979) in boxes of limited dimensions, because of the presence of lateral walls, as was observed also by Busse & Whitehead (1971).

A completely different form of this instability occurs in limited domain for the transition from large to lower wavenumbers. This instability was found experimentally for low and intermediate Pr ($Pr < 20$) by Kolodner *et al.* (1986) and was called *soft* in

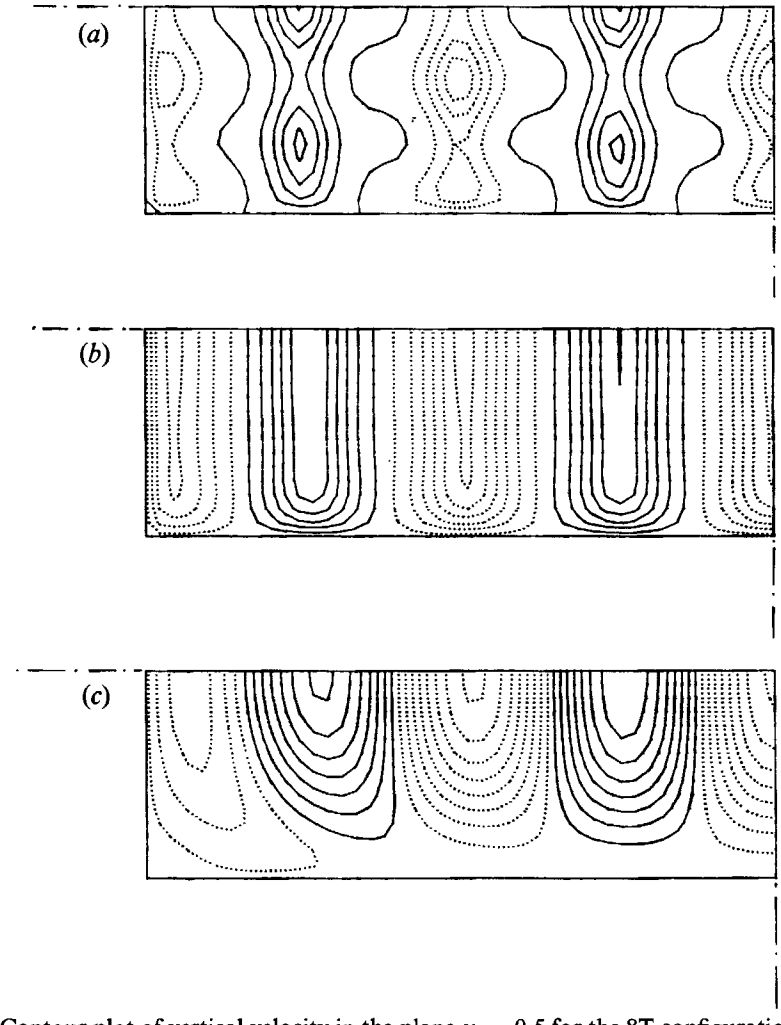

FIGURE 9. Contour plot of vertical velocity in the plane $x_2 = 0.5$ for the 8T configuration at $Pr = 15$. Continuous lines represent positive velocities and dashed lines represent negative velocities. Symmetry has been assumed in the computation and in the representation of the velocity field. (*a*) $Ra = 40000$, (*b*) $Ra = 10000$, (*c*) $Ra = 2000$.

the sense that the mean roll wavenumber can be varied continuously by stretching and squeezing the curved roll (figure 7). The numerical results presented in figure 7 validate, from a theoretical point of view, the experimental findings of Kolodner *et al.* (1986), that is that the soft-roll instability is similar to the skewed-varicose instability in that it is a quasi-steady transition from a configuration which is not stable at a particular Ra (e.g. 8T at $Ra = 5000$) to another configuration which is stable at that Ra. In fact we find a stable 8T solution at $Ra = 4000$ close to the skewed-varicose instability line. By increasing Ra, the stable solution reverts to a configuration which is inside the stable region (hatched area in figure 2) or on the boundary of the stable region, such as the soft roll at $Ra = 5000$ shown in figure 7. The solutions of figure 7 were obtained, as suggested by the experiments of Kolodner *et al.* (1986), by changing Ra in a quasi-steady way, starting from the soft-roll configuration at $Ra = 5500$. The wavenumber

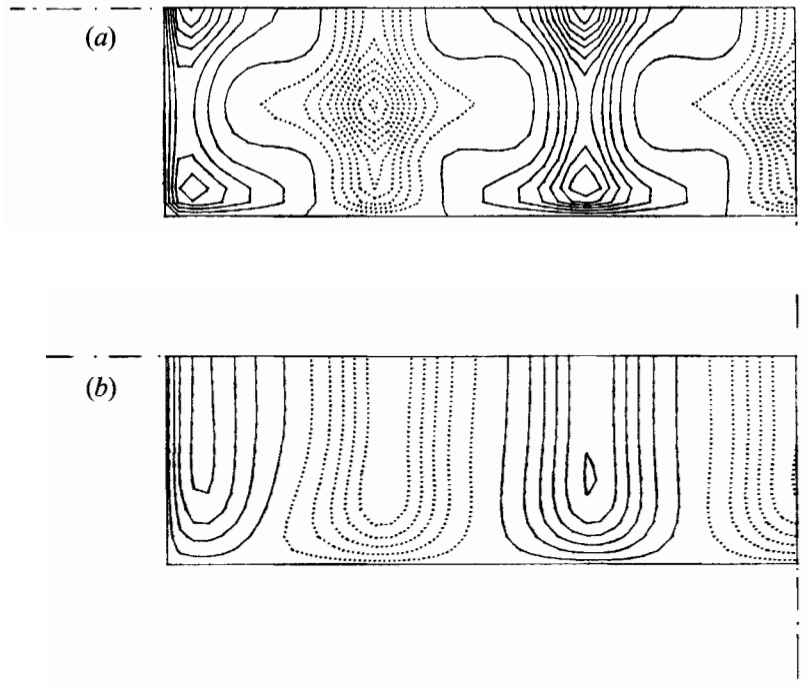

FIGURE 10. Contour plot of vertical velocity in the plane $x_2 = 0.5$ for the 6T configuration at $Pr = 15$. (Symmetry assumed.) (*a*) $Ra = 27500$, (*b*) $Ra = 7000$.

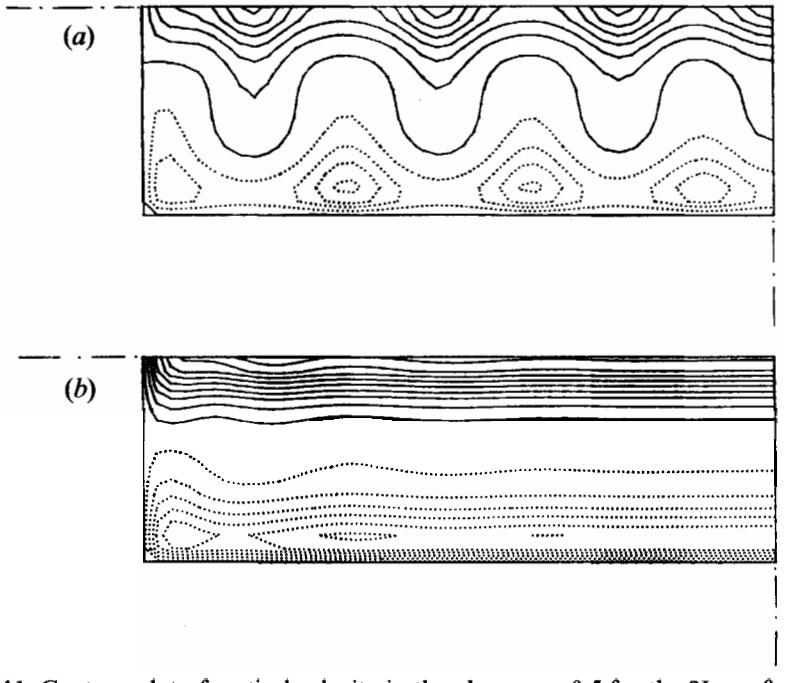

FIGURE 11. Contour plot of vertical velocity in the plane $x_2 = 0.5$ for the 2L configuration at $Pr = 15$. (Symmetry assumed.) (*a*) $Ra = 25000$, (*b*) $Ra = 20000$.

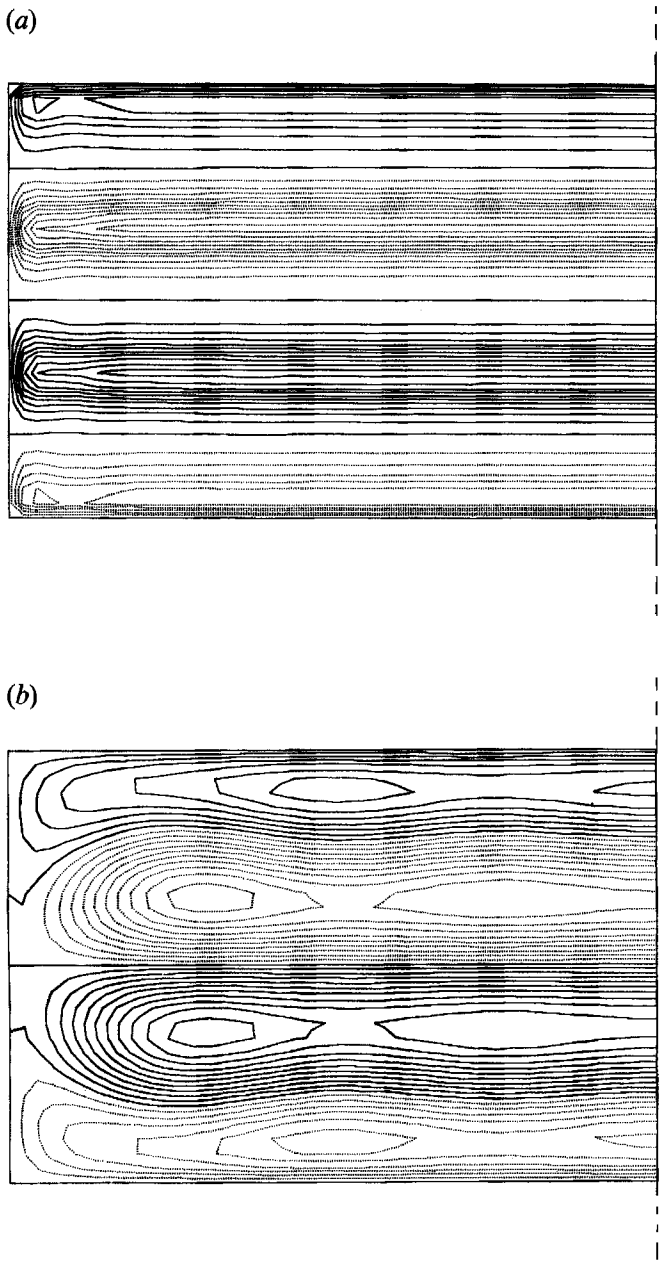

FIGURE 12. Contour plot of vertical velocity in the plane $x_2 = 0.5$ for the 3L configuration at $Pr = 15$. (Symmetry assumed.) (*a*) $Ra = 40\,000$, (*b*) $Ra = 2000$.

α of the central rolls increases with decreasing Ra, as shown by the soft-roll behaviour (figure 2). For $Ra < 3000$ the soft-roll structure becomes unstable and the 8T roll configuration is obtained.

It should be noted that at $Ra = 5000$, in contrast to all the other results analysed in this work, a complete mixing amongst the different rolls is present in the soft-roll

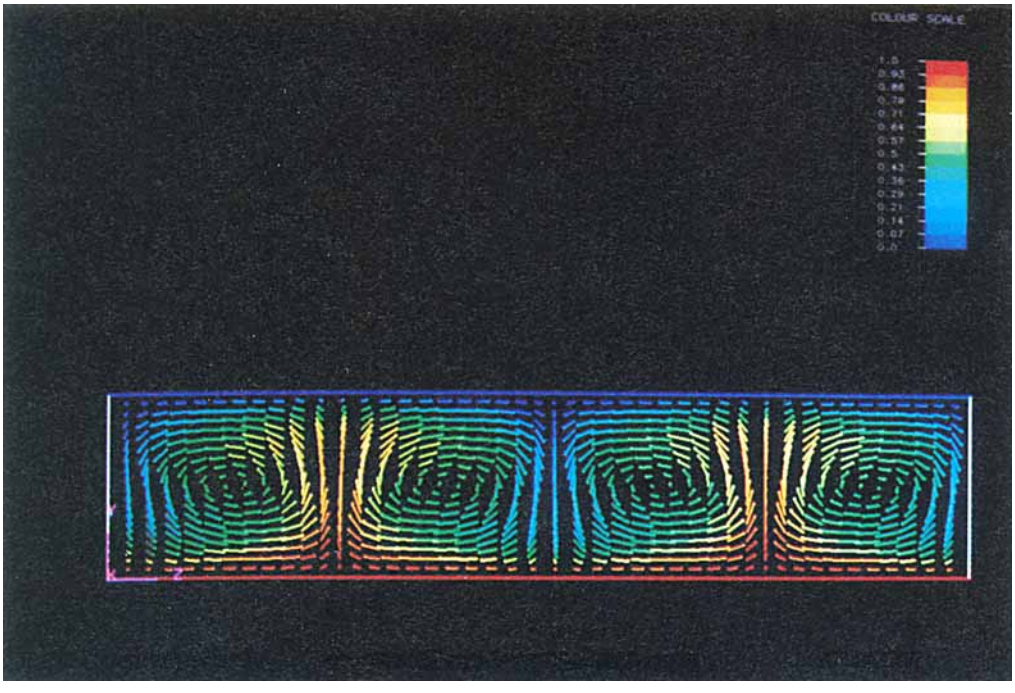

FIGURE 13. Velocity vectors on the symmetry plane perpendicular to the transverse rolls ($x_1 = 1.5$) for the 8T configuration at $Ra = 10000$ and $Pr = 15$. The colour indicates the temperature of the fluid. (Symmetry assumed.)

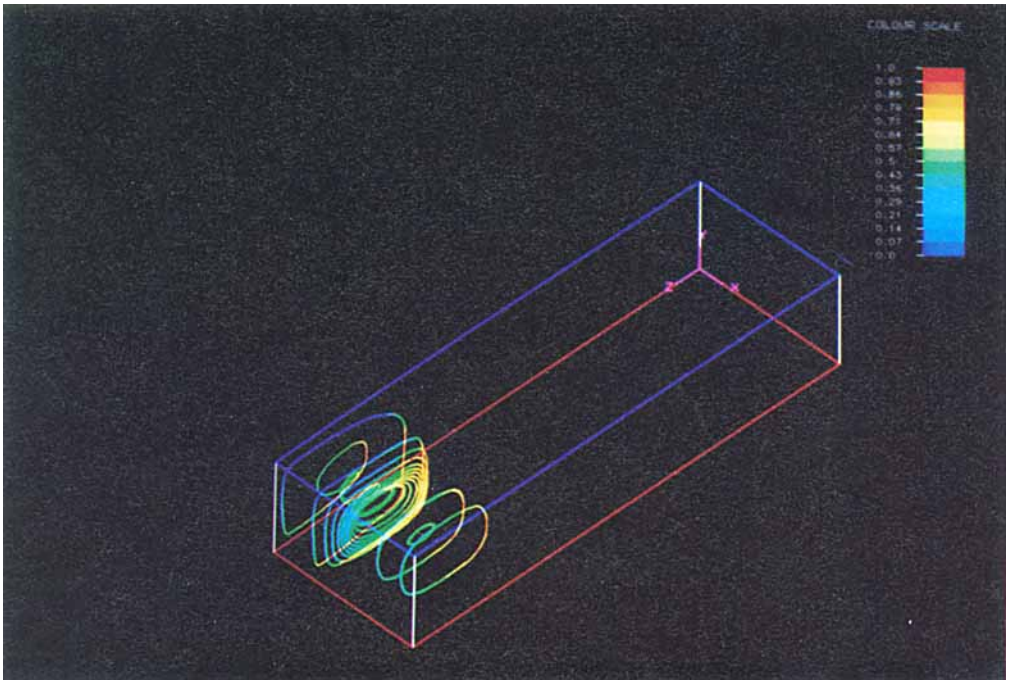

FIGURE 14. Pathlines for the quasi-two-dimensional base flow at $Ra = 10000$ and $Pr = 15$. (Symmetry assumed.)

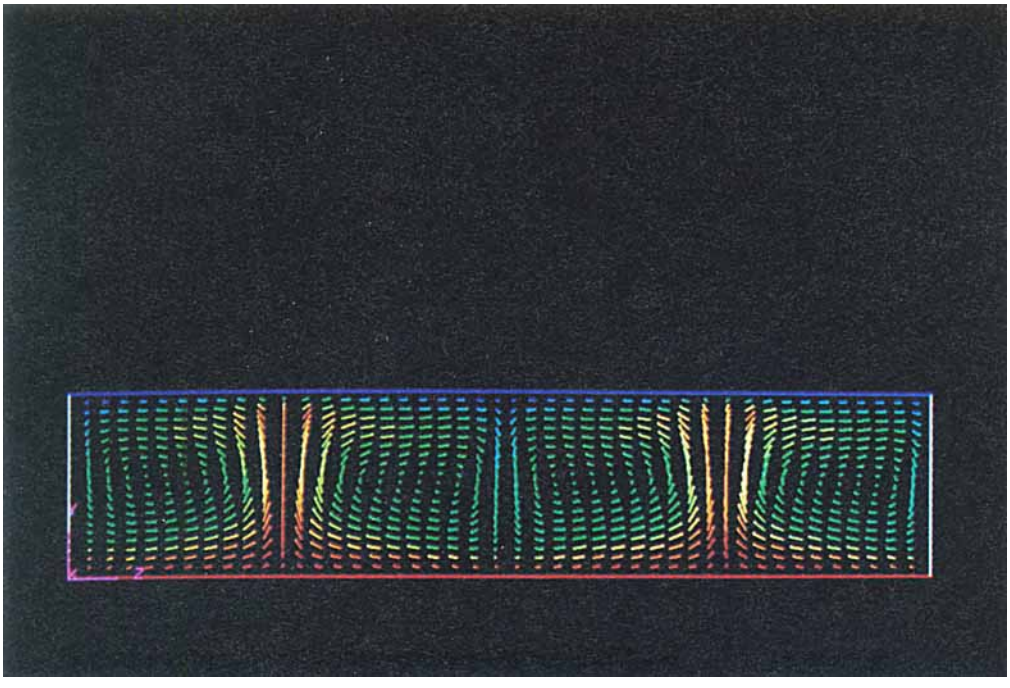

FIGURE 15. Velocity vectors on the symmetry plane perpendicular to the main rolls ($x_1 = 1.5$) for the 8T configuration at $Ra = 40000$ and $Pr = 15$. (Symmetry assumed.)

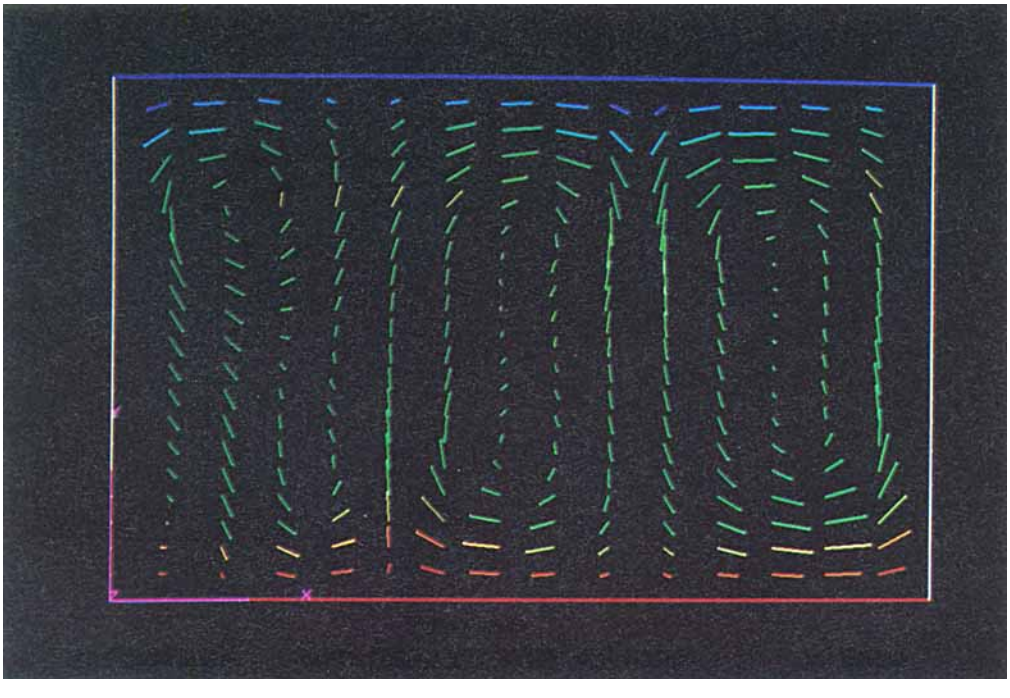

FIGURE 16. Velocity vectors, showing the cross-rolls on the plane containing the axis of the fourth main roll ($x_3 = 3.9$) for the 8T configuration at $Ra = 40000$ and $Pr = 15$. (Symmetry assumed.)

configuration, as may be seen in the particle track shown in figure 8.† In fact, a particle released at a point very close to the lower wall is tracked in the bulk of the fluid and jumps from the curved roll to the straight transverse roll close to the symmetry plane.

The numerical results obtained indicate that the soft-roll structure is a very stable and robust flow configuration for the Rayleigh–Bénard problem in bounded domains. In fact this structure has been shown in the present numerical study to be insensitive to numerical discretization errors and small perturbations of initial conditions (e.g. see the mesh sensitivity analysis in §5.2), just as it has been insensitive to the experimental uncertainty in the construction of the test section and in the evaluation and control of physical properties of fluid and walls in the experiments by Kolodner *et al.* (1986).

An aspect which requires further explanation is the greater stability of the 3L configuration to the skewed-varicose structure (see figure 2). This is due to the straightening effect of the lateral walls, which also occurs at $Pr = 15$ (figure 3).

5.4. *Prandtl number* = 15

To correlate the present numerical results in a bounded domain with the experimental work of Kolodner *et al.* (1986) and to permit a comparison with the stability studies of Busse & Clever (1979), $Pr = 15$ (corresponding to ethanol at a temperature of 30 °C) was selected. From figure 3 (see also figure 3 of Busse & Clever 1979) it is evident that for $Pr = 15$, the cross-roll configuration and skewed-varicose instability may both be possible: the first one is associated with the lower wavenumbers, the second with the higher wavenumbers.

5.4.1. *Quasi-two-dimensional configurations*

First we focus our attention on the quasi-two-dimensional base flow configurations which occur for values of Ra and α corresponding to the hatched area of figure 3. As previously discussed for a bounded domain, only a finite multiplicity of solutions is possible, due to the discretization of the wavenumber. These are shown in table 2, where we present the results obtained for 8T, 6T, 3L and 2L configurations.

In figures 9, 10, 11 and 12 contour plots of vertical velocity in the mid-horizontal plane ($x_2 = 0.5$) for the configurations 8T, 6T, 2L and 3L respectively are shown. The basic 8T pattern which can be seen is observed near the onset of motion (figure 9) remain stable up to $Ra = 32000$. This value seems to fit quite well with the theoretical prediction (figure 3). An example of the motion in the quasi-two-dimensional configuration is illustrated in figure 13, which shows the velocity vectors on the symmetry plane at $Ra = 10000$. The change in shape of the end rolls, which is particularly evident at small Ra (figure 9), results from the increase of the kinematic boundary-layer thickness near the lateral wall. As expected from the stability analysis for an infinite fluid layer (figure 3), the solution is two-dimensional in the bulk of the fluid domain, as is illustrated by the tracks of particles released near the symmetry plane (figure 14). Note that these tracks represent a minimum of twenty revolutions

† The choice of the proper algorithm for integration of particle tracks has been a significant difficulty in order to obtain accurate trajectories. We have obtained the best results using a fourth-order Runge–Kutta algorithm for time integration and a local third-order interpolation for space representation of velocity. Two type of tests have been used to check the accuracy obtained: (i) Several very long tracks were generated (up to 1 000 000 time steps), and using the final positions as starting point reverse tracks were calculated so as to return to the initial point. The relative error evaluated as the non-dimensional distance between the first and the final point was less than 10^{-6}. (ii) Closed path lines have been generated in planes with two-dimensional flows; after a large number of loops (20–25) the relative error was less than 10^{-7}.

around the axis of the roll. The only three-dimensional motion which occurs is confined to a region close to the endwall where a spiralling movement is present, in the form discussed by Mallinson & de Vahl Davis (1977). Analogous behaviour occurs in all the other base configurations, up to the *Ra* value for the transition to the cross-roll structure (see table 2).

5.4.2. *Cross-roll*

The infinite stability analysis (figure 3) indicates that, depending on value of the wavenumber, the transition to the cross-roll structure for numerical solutions may occur in two different ways: direct for $\alpha < a_l$; or passing through the skewed-varicose instability region for $\alpha > a_l$, where $\alpha_l \approx 2.8$ is the wavenumber corresponding to the intersection of the cross-roll and skewed-varicose instability lines.

In fact, for $\alpha < \alpha_l$ it is possible to have an *Ra* larger than the stability boundary predicted in the infinite domain (cross-roll line in figure 3) and retain the cross-roll structure (table 2). The presence of cross-roll structure is detected using the isovels of figures 9–12. In the bimodal structure the vorticity associated with the two orthogonal systems of rolls (base-rolls configuration and cross-rolls) is of the same order of magnitude. These structure are represented by filled symbols in figure 3. Very distorted flow structures are obtained (figures 9, 10 and 11). These numerical results, which are in qualitative agreement with the experimental findings of Kolodner *et al.* (1986), may be interpreted (as was mentioned by Busse & Whitehead 1971) as a gravitational instability of the upper and lower thermal boundary layers, which occurs because insufficient heat is transported by the base rolls to reduce the thickness of the thermal boundary layer sufficiently. The cross-roll wavenumber (presented in table 2) decreases with decreasing *Ra* and is in qualitative agreement with the predictions of α_c made by Busse & Whitehead (1971) in the (α, α_c)-plane, even though the continuous curves presented by Busse & Whitehead (1971) are reduced to points due to the discretization of α_c as well as α in bounded domains.

In figures 15 and 16 the velocity vectors for the 8T configuration at $Ra = 40000$ are shown on the symmetry plane perpendicular to the main rolls and in a plane containing the axis of the fourth main roll. The presence of six cross-rolls is clearly seen in figure 16; this structure corresponds to $\alpha_c = 6.28$. The effect of convection on the temperature field is demonstrated by the dimension of the hot plume (red and orange vectors) in the upward flow region.

The cross-roll instability for the base 6T configuration, shown in figure 10, grows at a value of *Ra* ($15000 < Ra < 20000$) which is smaller than that for the 8T configuration. This critical *Ra* is again in good agreement with the value predicted for an infinite domain for the transition to the cross-roll (figure 3). There are four cross-rolls in this case, corresponding to a wavenumber of 4.18.

For the 2L configuration the cross-roll instability is encountered at a higher Rayleigh number ($20000 < Ra < 25000$) (figure 11), the number of cross-rolls is 14 and the two rolls close to the symmetry plane are smaller than the other twelve. The critical *Ra* for the 2L configuration is larger than for 6T even though they both have the same main wavenumber. This larger value can be explained by the stabilizing effect of the lateral walls to the cross transverse rolls (endwall effect).

The behaviour of the 3L configuration is different from that of the other three, as may be seen in figure 12. The quasi-two-dimensional solution remains stable up to $Ra = 40000$, which is well above the skewed-varicose instability line from the infinite domain (figure 3). A similar result is also found for $Pr = 0.71$ for this configuration.

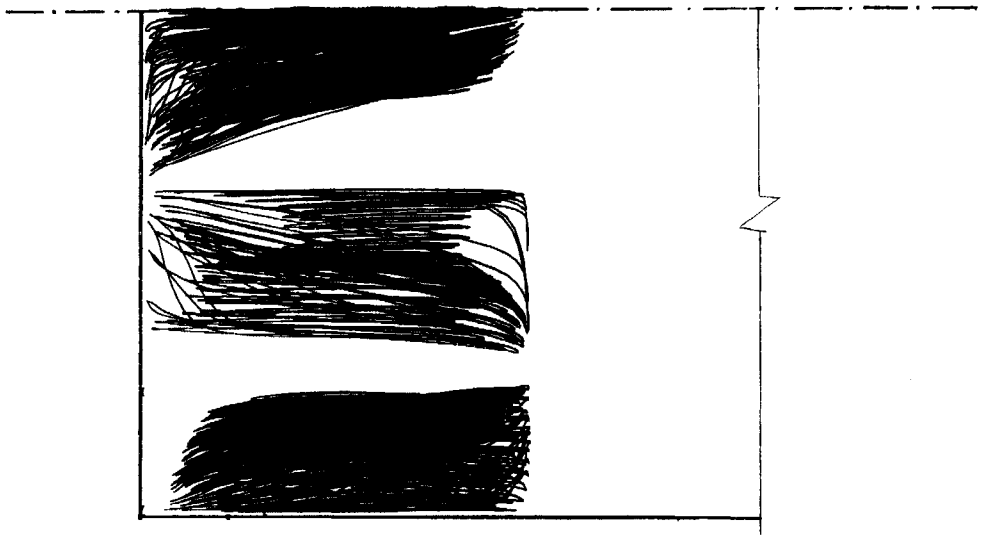

FIGURE 17. Tracks of particles released in three different regions of the first roll for the 8T configuration at $Ra = 40000$ and $Pr = 15$, showing the segmentation of the main roll due to the cross-rolls. (Symmetry assumed.)

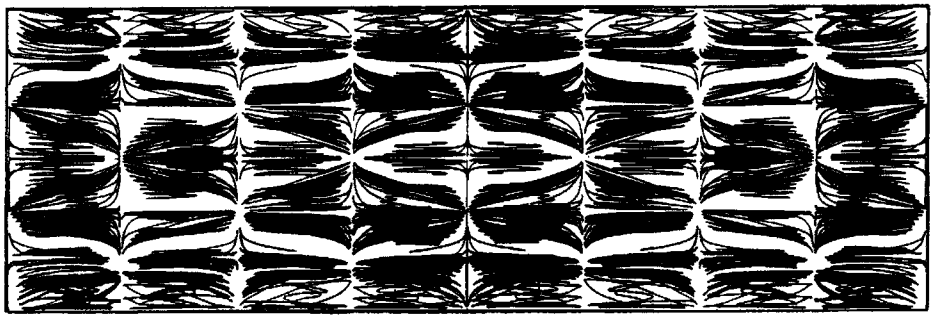

FIGURE 18. Tracks of particles released in 48 different regions for the 8T configuration at $Ra = 40000$ and $Pr = 15$ showing the inclination of the paths.

Furthermore for $Ra = 2000$, which is on the lower branch of the cross-roll stability line, a flow structure with weak cross-rolls is obtained. This phenomenon is not observed for the other three configurations for Ra on the lower branch of the stability line of the cross-roll.

An important aspect of the cross-roll structure, which is illustrated by the particles tracks shown in figure 17, is not only the complete absence of mixing among the rolls but also the segmentation of each main roll into subregions, in which the fluid particles remain. The three-dimensional nature of the flow and the cross-roll effect is evident from the inclination of the trajectories within the confined subregions. There is no mass transfer from one subregion to another even after hundreds of revolutions of the particle tracks. The tracks of a large number of particles released at the same time in all the 48 different regions determined by the intersection of the main and the cross-rolls are shown in figure 18. The qualitative overall behaviour of the particle tracks is in agreement with that found experimentally by Willis (figure 8 of Busse & Whitehead 1971) in the case of bimodal convection.

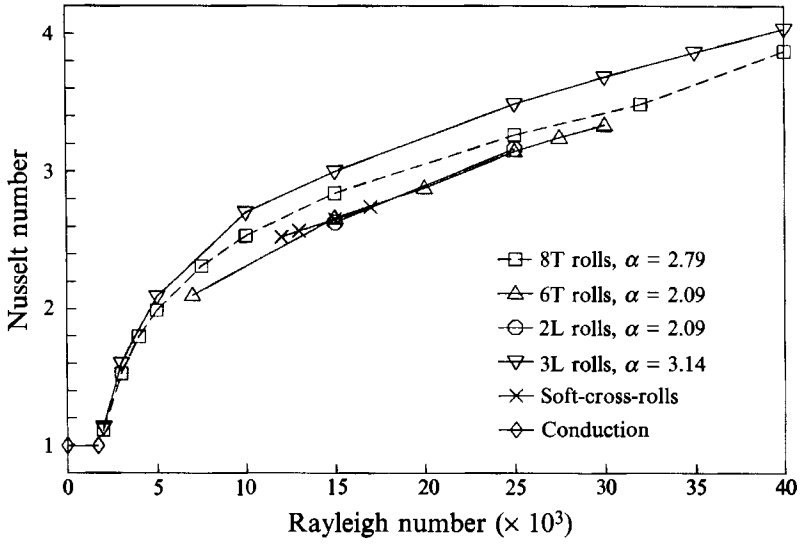

FIGURE 19. *Nu vs. Ra* for $Pr = 15$. The numerical uncertainty is estimated to be equal to 4% (see table 1 and figure 5).

5.4.3. *Soft roll*

In the same way as for a box filled with a fluid with $Pr = 0.71$ the skewed-varicose instability is detected in bounded domains filled with a fluid with $Pr = 15$ in the form of the soft roll structure. A peculiar characteristic at $Pr = 15$ is that the soft roll drives the transition to cross roll instability (figure 3) instead of to oscillatory instability, as in the case at $Pr = 0.71$. Therefore at increasing Ra the flow structure shows a transition from a standard soft roll solution to a more complex structure that exhibits the coexistence of soft- and cross-roll structures. The soft roll structure is found in the Ra range ($12000 < Ra < 17000$). In figure 4(*a*) the isovels at $Ra = 12000$ show the standard soft-roll configuration, which at $Ra = 15000$ changes into a soft-cross-roll (SCR) configuration. A picture showing this configuration at $Ra = 17000$ may be seen in figure 4(*b*). For these configurations, owing to the presence of the cross-roll pattern, it is not possible to give a meaningful evaluation of the wavenumber α. Thus these results are not reported on the skewed-varicose instability line of figure 3.

Therefore for the configurations considered, which are also all the possible configurations according to the stability diagrams in figure 3, good agreement is found with Busse & Clever (1979) and Kolodner *et al.* (1986) in the form of the instability at large Ra and in the value of the critical Ra for the transition to the cross-roll and soft-roll structures. Furthermore the cross-roll configurations seem to remain stable up to the onset of the unsteady oscillatory solution (Ra_{II}). On the other hand, owing to the presence of the lateral walls, we do not find the zig-zag instability in the lower region of figure 3.

5.5. *Heat transfer*

In the quasi-two-dimensional structure, the rate of heat transfer is a maximum for rolls of nearly square cross section ($\alpha \approx 3.14$), as observed by Kolodner *et al.* (1986). Therefore a solution with α different from 3.14 (e.g. $\alpha = 2.09$ for 6T) gives a smaller rate of heat transfer as may be seen in figure 19 ($Pr = 15$). The lower curves correspond to the structures with wavenumber $\alpha = 2.09$ (6T and 2L). The upper curve corresponds to the 3L configuration which has $\alpha = 3.14$.

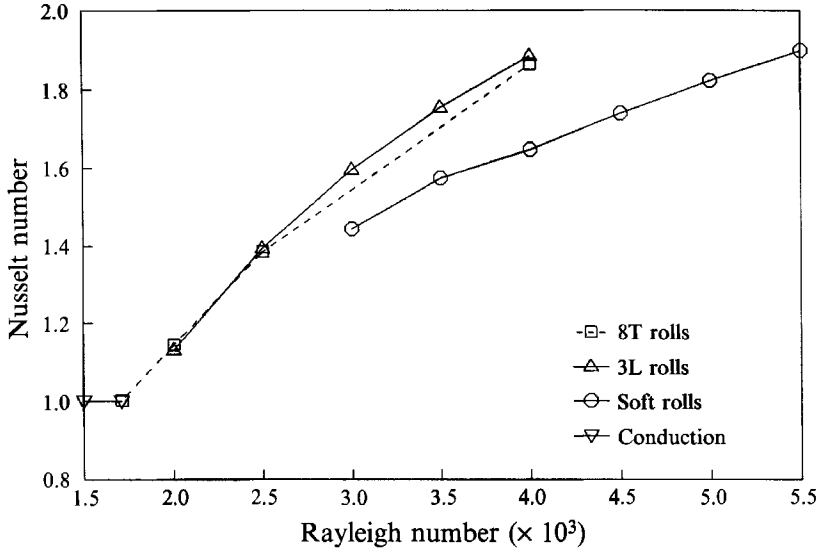

FIGURE 20. *Nu vs. Ra* for $Pr = 0.71$.

Furthermore, as discussed by Busse & Whitehead (1971), the bimodal convection increases the rate of heat transfer over that of the base single mode. In fact, as shown by figure 19, there is a slight change in the slope of the curve of the 8T configuration with the growth of the cross-rolls.

The phenomenon of the multiple *Nu vs. Ra* curves, for the quasi-two-dimensional solutions is less clear for $Pr = 0.71$ (figure 20); this is due to the thinner stability region and lower *Nu* values ($Nu < 2$). As may be seen in figure 20, a lower value of *Nu* is obtained for the soft-roll configuration, in agreement with the experimental findings of Kolodner *et al.* (1986). These multiplicities in the heat transfer curves may in some way explain the abnormal behaviour of *Nu vs. Ra* found experimentally by Kennedy & Gani (1987).

6. Conclusions

The numerical simulation of the convection flows in closed boxes yields interesting information on the steady flow structures and the types of spatial instability occurring in the supercritical *Ra* regime ($Ra_I < Ra < Ra_{II}$). In particular the present study validates the use of the infinite-domain analysis (Busse & Clever 1979; Clever & Busse 1974) to predict the onset and types of instabilities, and confirms the experimental investigations in limited domains of Kolodner *et al.* (1986).

The main conclusions are:

(i) For low and intermediate *Ra* a multiplicity of steady solutions of *quasi-two-dimensional* type have been found. For these flow structures, different *Nu vs. Ra* curves are obtained, where the largest values of *Nu* are associated with the wavenumbers closest to square rolls. Comparisons with the experiments of Kolodner *et al.* (1986) for two structures (8T, 10T) give good quantitative agreement (maximum error less than 4%).

(ii) For large *Ra* two types of steady instabilities have been obtained: the *cross-roll* (for $Pr = 15$) and the *soft-roll* (for $Pr = 0.71$ and 15). The computed values of critical *Ra* as a function of wavenumber α for the transition to a cross-roll accurately fit the

theoretical curves shown by Kolodner *et al.* (1986) for infinite domain for the three possible structures with $\alpha < 2.8$ (8T, 6T, 2L). For $\alpha > 2.8$ (3L) we did not find the cross-roll instability for increasing *Ra*, in agreement with the results of Kolodner *et al.* (1986), and the quasi-two-dimensional structure seems to remain stable for *Ra* values above those required to cause the skewed-varicose instability in an infinite domain. For the 3L configuration we found a weak cross-roll in the lower branch of the theoretical stability line. The cross-roll leads to bimodal convection for increasing *Ra*. The numerical solutions show a fully three-dimensional flow field, in which mixing and mass flux are located within subregions bounded by each main and cross-roll. Although bimodal convection increases the rate of heat exchange, the change in slope of the *Nu v. Ra* curve is barely perceptible.

The soft-roll (or skewed-varicose) instability at low and intermediate *Pr* ($Pr = 0.71$ and 15) is a steady mechanism for the transition from structures with one wavenumber to those with a different wavenumber corresponding to a solution which does not violate the stability constraints. For $Pr = 0.71$, the soft-roll instability leads to oscillatory solutions. The wavenumbers evaluated from these results follow quite well the skewed-varicose instability line in unlimited domains (Busse & Clever 1979). Therefore it seems that the soft-roll and the varicose instabilities are two expressions of the same steady instability. For $Pr = 15$ the soft-roll leads to the cross-roll structure and the flow appears as the combination of the two flow patterns.

(iii) The lateral walls have a stabilizing effect on the zig-zag and varicose instability.

The authors thank Professor G. de Vahl Davis and Professor J. A. Reizes for their helpful suggestions in the progress of the present research.

A major portion of this work has been part of the PhD dissertation submitted by F. Stella in fulfilment of the requirements for the PhD degree in Applied Mechanics at the University of Rome (Stella 1989).

REFERENCES

BÉNARD, H. 1900*a* Les tourbillons cellulaires dans une nappe liquide. *Rev. Gén. Sci. Pures Appl.* **11**, 1261–1271.

BÉNARD, H. 1900*b* Les tourbillons cellulaires dans une nappe liquide. *Rev. Gén. Sci. Pures Appl.* **11**, 1309–1328.

BOLTON, E. W., BUSSE, F. H. & CLEVER, R. M. 1983 An antisymmetric oscillatory instability of convection rolls. *Bull. Am. Phys. Soc.* **28**, 1399.

BOLTON, E. W., BUSSE, F. H. & CLEVER, R.M. 1986 Oscillatory instabilities of convection rolls at intermediate Prandtl numbers. *J. Fluid Mech.* **164**, 469–485.

BUSSE, F. H. 1967*a* On the stability of two-dimensional convection in a layer heated from below. *J. Math. Phys.* **46**, 140–150.

BUSSE, F. H. 1967*b* Non-stationary finite amplitude convection. *J. Fluid Mech.* **28**, 223–239.

BUSSE, F. H. 1978 Non-linear properties of thermal convection. *Rep. Prog. Phys.* **41**, 1929–1967.

BUSSE, F. H. & CLEVER, R. 1979 Instabilities of convection rolls in a fluid of moderate Prandtl number. *J. Fluid Mech.* **91**, 319–335.

BUSSE, F. H. & WHITEHEAD, J. A. 1971 Instabilities of convection rolls in a high Prandtl number fluid. *J. Fluid Mech.* **47**, 305–320.

CLEVER, R. & BUSSE, F. H. 1974 Transition to time-dependent convection. *J. Fluid Mech.* **65**, 625–645.

DAVIES-JONES, R. P. 1970 Thermal convection in an infinite channel with no-slip condition. *J. Fluid Mech.* **44**, 695–704.

DAVIS, S. H. 1967 Convection in a box: linear theory. *J. Fluid Mech.* **30**, 465–478.

FRICK, H., BUSSE, F. H. & CLEVER, R. 1983 Steady three-dimensional convection at high Prandtl numbers. *J. Fluid Mech.* **127**, 141–153.

GUJ, G. & STELLA, F. 1988 Numerical solution of high-*Re* recirculating flows in vorticity-velocity form. *Intl J. Numer. Meth. Fluids* **8**, 405–416.

GUJ, G. & STELLA, F. 1993 A vorticity–velocity method for the numerical solution of 3D incompressible flows. *J. Comput. Phys.* **106**, 286–298.

JOSEPH, D. D. 1976 *Stability of Fluid Motion*, vol. 1, Springer.

KENNEDY, J. & GANI, R. 1987 Effect of aspect ratio on natural convection in rectangular enclosures. In *Second Workshop on Natural Convection in Enclosures*, pp. 32–35. University of New South Wales.

KESSLER, R. 1987 Nonlinear transition in three-dimensional convection. *J. Fluid Mech.* **174**, 357–379.

KIRCHARTZ, K. & OERTEL, H. 1988 Three-dimensional thermal cellular convection in rectangular boxes. *J. Fluid Mech.* **192**, 249–286.

KOLODNER, P., WALDEN, R., PASSNER, A., SURKO, C. 1986 Rayleigh–Bénard convection in an intermediate-aspect-ratio rectangular container. *J. Fluid Mech.* **163**, 195–226.

KRISHNAMURTI, R. 1970 On the transition to turbulent convection. Part 2. The transition to time-dependent flow. *J. Fluid Mech.* **42**, 309–320.

LANDAU, L. D. & LIFSHITZ, E. M. 1975 *Fluid Mechanics*, 6th Edn. Pergamon.

MALLINSON, G. & DE VAHL DAVIS, G. 1973 The method of the false transient for the solution of coupled elliptic equations. *J. Comput. Phys.* **12**, 435–461.

MALLINSON, G. & DE VAHL DAVIS, G. 1977 Three dimensional natural convection in a box: a numerical study. *J. Fluid Mech.* **83**, 1–31.

MAURER, J. & LIBCHABER, A. 1979 Rayleigh–Bénard experiment in liquid helium; frequency locking and the onset of turbulence. *J. Phys. Lett. Paris* **41**, L515-L518.

MOTSAY, R. W., ANDERSON, K. E. & BEHRINGER, R. P. 1988 The onset of convection and turbulence in rectangular layers of normal liquid He. *J. Fluid Mech.* **189**, 263–286.

RAYLEIGH, LORD 1916 On convective currents in a horizontal layer of fluid when the higher temperature is on the underside. *Phil. Mag.* **32**, 529–546.

SAMARSKII, A. & ANDREYEV, V. 1963 On a high-accuracy difference scheme for elliptic equation with several space variables. *USSR Comput. Maths. Math. Phys.* **3**, 1373–1382.

STELLA, F. 1989 Problema di Rayleigh–Bénard in domini limitati. PhD thesis, Università degli Studi di Roma 'La Sapienza'.

STELLA, F. & GUJ, G. 1989 Vorticity–velocity formulation in the computation of flows in multiconnected domains. *Intl J. Numer. Meth. Fluids* **9**, 1285–1298.

STELLA, F., GUJ, G., LEONARDI, E. & DE VAHL DAVIS, G. 1988 The velocity–vorticity and the vector potential–vorticity formulation in three-dimensional natural convection. *Rep.* 1988/FMT/4. University of New South Wales ISBN 0156 3068.

STORK, K. & MÜLLER, U. 1972 Convection in a box: experiments. *J. Fluid Mech.* **54**, 599–611.